Finite element analysis of a bubble absorber

K.S. Sujatha, A. Mani and S. Srinivasa Murthy
Department of Mechanical Engineering, Indian Institute of Technology, Madras, India

Received January 1996
Revised September 1996

Nomenclature

A	= area, m^2
c	= concentration, –
D	= diameter, m
Dc	= diffusion coefficient, $m^2.s^{-1}$
f	= friction factor, m^{-1}
G	= conductance, $kg.m^{-2}.s^{-1}$
g	= gravitational constant, $m.s^{-2}$
h	= specific enthalpy, $J.kg^{-1}$
k	= average heat transfer coefficient, $W.m^{-2}.K^{-1}$
$k_L a$	= volume mass transfer coefficient, $kg.m^{-3}.s^{-1}$
$\dot{m}$	= mass flow rate, kg.s–1
m	= mass flux, $kg.m^{-2}.s^{-1}$
p	= pressure, $N.m^{-2}$
Q	= heat flux density, $W.m^{-3}$
T	= temperature, K
t	= time, s
v	= specific volume, $m^3.kg^{-1}$
w	= velocity, $m.s^{-1}$
x	= dryness fraction, –
z	= space coordinate, m

Greek symbols

α	void fraction, –
λ	heat transfer coefficient, $W.m^{-2}.K^{-1}$
μ	dynamic viscosity, $kg.m^{-1}.s^{-1}$
ξ	concentration, –
ρ	density, $kg.m^{-3}$
σ	mass density flow rate, s^{-1}
υ	kinematic viscosity, $m^2.s^{-1}$
ψ	angle of inclination, –

Subscripts

0	inlet
1	liquid
2	gas
cw	cooling water
G	gas
gen	generated
L	liquid
la	liquid absorbent
lr	liquid refrigerant

Introduction

Proper understanding of the heat and mass transfer in absorbers is necessary owing to their wide applications in refrigeration and chemical industries. Experimental investigations on heat and mass transfer in vertical tubular bubble absorbers used in refrigeration systems are usually limited because of high operating pressures. Therefore, numerical investigations are essential for a thorough understanding.

In the vertical tubular bubble absorber, the weak solution is supplied at the lower end of an array of tubes and the gas which bubbles into the solution is absorbed gradually and the concentrated solution is obtained at the upper end of the tubes. The heat of absorption is removed by circulating coolant.

Several investigators (Jagota *et al.*, 1973; Kasturi and Stepanek, 1974; Shilimkan and Stepanek, 1977) have experimentally studied cocurrent mass transfer in horizontal as well as vertical tubes. Kouremenos *et al.* (1990, 1993) have analysed heat and mass transfer in neutral gas absorption refrigeration

The authors thank the Council of Scientific and Industrial Research, Government of India for sponsoring a project on the development of transfer tank operated vapour absorption refrigeration system. This work forms a part of the above project.

International Journal for Numerical Methods for Heat & Fluid Flow
Vol. 7 No. 7, 1997, pp. 737–750.

units. They have developed a model for simulation of absorption process in a neutral gas absorption refrigeration unit using methylamine as refrigerant and hydrogen as inert gas. Heat and mass transfer analyses are carried out by solving the differential equations expressing the transport of momentum, heat and mass by finite difference technique. Variations in velocity, temperature and concentration and the overall heat and mass transfer characteristics of absorption process are analysed in detail.

Theoretical and experimental studies on the vertical tubular bubble absorber are scarce owing to the complex heat and mass transfer processes. Keizer (1982) and Infante Ferreira *et al.* (1984) have investigated vertical tubular bubble absorbers used in vapour absorption refrigeration systems. They have performed experiments on bubble absorbers with different heights and diameters using ammonia and water as the working fluid and have proposed a correlation for the design of an absorber.

In the present work, heat and mass transfer in the cocurrent vertical tubular absorber has been numerically investigated. The analysis is based on the theoretical works of Schittke (1975) and Soo (1967). The equations are solved using the finite element method employing Galerkin's technique (Prashanth and Seetharamu, 1993; Segerlind, 1984). The results have been validated with Keizer's (1982) experimental data for ammonia-water system. Using this model, the performance of tubular absorbers working with R22-DMF as working fluid are presented in this paper. The volumetric mass transfer coefficient expressed through Sherwood number is correlated to the Reynolds number, Schmidt number and length to diameter ratio.

Governing equations

Figure 1 shows the physical model of the vertical tubular bubble absorber. The description of the state of a flowing medium is done by using the fundamental conservation laws for mass, energy and momentum leading to a set of partial differential balance equations. In the present case, it is assumed that the system is in thermodynamic equilibrium at every moment. Though this assumption is not valid for the description of phase change processes, it presents a sensible approximation of sufficient accuracy. The governing partial differential equations (Schittke, 1975) are discussed below.

Continuity equation

The mass balance of the mixture is

$$\frac{Dv}{Dt} = v \frac{\partial w}{\partial z} \tag{1}$$

where v is the mean specific volume of the mixture given by

$$v = v_1 + x\, v_{21} \tag{2}$$

$$v_{21} = v_2 - v_1 \tag{3}$$

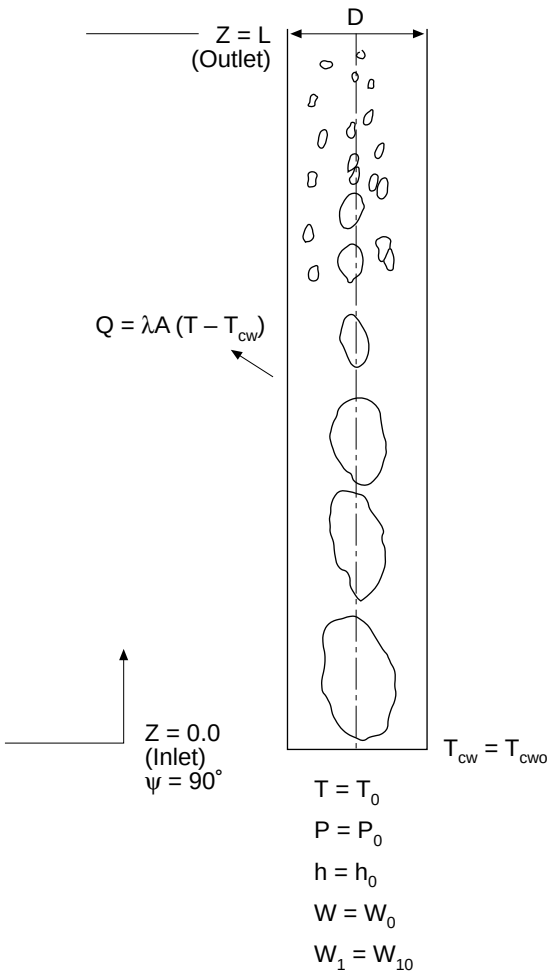

Figure 1.
Physical model of the tubular absorber

x is the dryness fraction. Since the liquid phase is a mixture containing liquid refrigerant and absorbent, the specific volume of the liquid phase v_1 is written as

$$v_1 = c\, v_{lr} + (1-c)\, v_{la} \tag{4}$$

where c is the concentration which represents the weight fraction of the refrigerant in the solution. The mean mixture velocity w is given by

$$w = w_1 + x\, w_{21} \tag{5}$$

$$w_{21} = w_2 - w_1 \tag{6}$$

Momentum equations

The mixture momentum balance equation is

$$\frac{Dw}{Dt} = -v \frac{\partial p}{\partial z} - g \sin \psi - fw^2 \quad (7)$$

where

$$fw^2 = (1-x) f_1 w_1^2 + x f_2 w_2^2 \quad (8)$$

f_1 and f_2 are the equivalent single phase friction factors depending on Reynolds number and the correlations are taken from Collier (1980).

The momentum balance equations for each of the two phases are written as

$$\frac{Dw_1}{Dt} = -v_1 \frac{\partial p}{\partial z} - (w_1 - w) \frac{\partial w}{\partial z} - g \sin \psi - f_1 w_1^2 + \sigma w_2 \quad (9)$$

$$\frac{Dw_2}{Dt} = -v_2 \frac{\partial p}{\partial z} - (w_2 - w) \frac{\partial w}{\partial z} - g \sin \psi - f_2 w_2^2 - \sigma w_2 \quad (10)$$

for the liquid and gaseous phases respectively.

Of the equations (9) and (10), equation (9) is solved along with the mixture momentum equation and for the other phase, velocity can be calculated using equations (5) and (6).

If σ represents mass density flow rate (Schittke, 1975) defining absorption from the gaseous phase to the liquid phase, the mass balance for the gaseous phase written in terms of dryness fraction is

$$\frac{\partial x}{\partial t} + w \frac{\partial x}{\partial z} = -\sigma \quad (11)$$

Energy equation

$$\frac{Dh}{Dt} = v Q + v \frac{Dp}{Dt} \quad (12)$$

where

$$h = h_1 + x h_{21} \quad (13)$$

$$Q = Q_{gen} - Q_{cw} \quad (14)$$

Q is the heat flux density induced by cooling water, Q_{gen} is the heat generated and Q_{cw} is the heat carried away by the coolant.

Thermodynamic and transport properties of working fluids used in the calculations are taken from the literature (Gallant, 1969). Fatouh and Srinivasa Murthy (1993a, 1993b, 1993c) presented P-T-X data for nine combinations of R22-absorbent solutions and heat of mixing data for R22 with six absorbents in the form of correlations.

Finite element formulation

The governing partial differential equations are discretized using Galerkin's finite element method. One dimensional linear element with two nodes is used for the analysis. The variation of properties in the element is given by

$$\Phi = N_1\Phi_1 + N_2\Phi_2 = [N]\{\Phi\}.$$

Where N_1 and N_2 are the shape functions and Φ represents any property. In the present analysis the equations (1), (7), (9) and (12) are solved to find the distributions of w, h, p and w_1. In the present study, the variables are written as

$$\{w\} = [N]\{w\} \qquad \{p\} = [N]\{p\} \qquad \{h\} = [N]\{h\}$$

$$\{v\} = [N]\{v\} \qquad \{fw^2\} = [N]\{fw^2\} \qquad \{w_1\} = [N]\{w_1\}$$

$$\{f_1w_1^2\} = [N]\{f_1w_1^2\}$$

The governing equations in the finite element form are

Continuity equation:

$$\int [N]^T \left(\frac{\partial v}{\partial t} + w\frac{\partial v}{\partial z} - v\frac{\partial w}{\partial z}\right) dz = 0 \tag{15}$$

Energy equation:

$$\int [N]^T \left(\frac{\partial h}{\partial t} + w\frac{\partial h}{\partial z} - vQ - v\frac{\partial p}{\partial t} - vw\frac{\partial p}{\partial z}\right) dz = 0 \tag{16}$$

Momentum equation of the mixture:

$$\int [N]^T \left(\frac{\partial w}{\partial t} + w\frac{\partial w}{\partial z} + v\frac{\partial p}{\partial z} + g\sin\psi + fw^2\right) dz = 0 \tag{17}$$

Momentum equation of the liquid phase:

$$\int [N]^T \left(\frac{\partial w_1}{\partial t} + w\frac{\partial w_1}{\partial z} + v_1\frac{\partial p}{\partial z} + w_1\frac{\partial w}{\partial z} - w\frac{\partial w}{\partial z} + g\sin\psi + f_1w_1^2 - \sigma w_2\right) dz = 0 \tag{18}$$

The final matrix form of the above equations is given by

$$\begin{bmatrix} K_{11}K_{12}K_{13}K_{14}K_{15}K_{16}K_{17}K_{18} \\ K_{21}K_{22}K_{23}K_{24}K_{25}K_{26}K_{27}K_{28} \\ K_{31}K_{32}K_{33}K_{34}K_{35}K_{36}K_{37}K_{38} \\ K_{41}K_{42}K_{43}K_{44}K_{45}K_{46}K_{47}K_{48} \\ K_{51}K_{52}K_{53}K_{54}K_{55}K_{56}K_{57}K_{58} \\ K_{61}K_{62}K_{63}K_{64}K_{65}K_{66}K_{67}K_{68} \\ K_{71}K_{72}K_{73}K_{74}K_{75}K_{76}K_{77}K_{78} \\ K_{81}K_{82}K_{83}K_{84}K_{85}K_{86}K_{87}K_{88} \end{bmatrix} \begin{Bmatrix} w_i \\ p_i \\ h_i \\ w_{2_i} \\ w_j \\ p_j \\ h_j \\ w_{2_j} \end{Bmatrix} = \begin{bmatrix} f_1 \\ f_2 \\ f_3 \\ f_4 \\ f_5 \\ f_6 \\ f_7 \\ f_8 \end{bmatrix} \tag{19}$$

The elements of the stiffness matrix are given in Appendix 1.

These equations are solved simultaneously in time and space with the following boundary and initial conditions.

At $z = 0$; $p = p_0$, $h = h_0$, $w = w_0$, $w_1 = w_{10}$

At $t = 0$; $p = p_0$, $h = h_0$, $w = w_0$, $w_1 = w_{10}$

Solution procedure

The inlet conditions of the gas and liquid are known. Inlet values are assigned as initial values for all the nodes. By solving the elemental matrix, the conditions at the second node are obtained. Since the elemental stiffness matrix and load vector involve unknown parameters at the second node of the same element (Prashanth and Seetharamu, 1993), the same conditions are assumed for both the nodes at the start of the iteration. With the new values obtained for node 2 during the first iteration, the next iteration is carried out. The iteration is continued until the values converge. Now the second node of the first element becomes the first node of the second element. The conditions at node 3 are evaluated in the same manner. In this way, the solution is marched forward until the end of the absorber is reached. Now the present values obtained at all the nodes become the initial values for the next time step. The solution procedure is repeated until the difference between values of successive time iterations is less than 10^{-5}. The time step is restricted to ensure numerical stability and is selected based on Courant number constraint.

The grid used for the present analysis is with 1401 nodes and the size of each element is 1.25mm. The suitability of this grid has been examined by comparing the different grids. One course mesh with 5mm element size and a very fine mesh with element size 0.5mm have been considered in addition to the present grid with 1.25mm. The difference in mass transfer coefficient calculated from the course and the present grid is greater than 25 per cent. On the other hand this difference is less than 1 per cent between the present and the fine grids. Therefore, the present grid with 1,401 nodes is adequate to carry out computations.

Results and discussion

The numerical code developed for the present analysis is validated with the available literature. The mass transfer coefficient (see Appendix 2) calculated from the present analysis using ammonia and water as working fluid has been compared with the experimental results of Keizer (1982). Table I shows the comparison and the agreement is found to be good.

Table I.
Comparison of mass transfer coefficients

Diameter (mm)	Height (m)	$k_L a$ (kg/m^3.3) Keizer (1982)	Present	Error (%)
10	1.75	94.528	85.27	10.8
15	1.75	122.87	113.43	8.3

A parametric study has been carried out with R22-DMF as working fluid in the present analysis. Figure 2 shows the variation of pressure along the height of the absorber for different diameters. The pressure drop near the leading end of the absorber is rapid owing to higher mass fraction. As the vapour gets absorbed along the height of the absorber, the mass fraction decreases and two-phase flow approaches single phase flow. This leads to a decrease in the rate of pressure drop as the flow proceeds towards the trailing end of the absorber. The figure also shows the effect of tube diameter. Two-phase pressure drop increases as the diameter decreases. Figure 3, which shows the variation of pressure drop against the diameter for different gas velocities, also supports the above results.

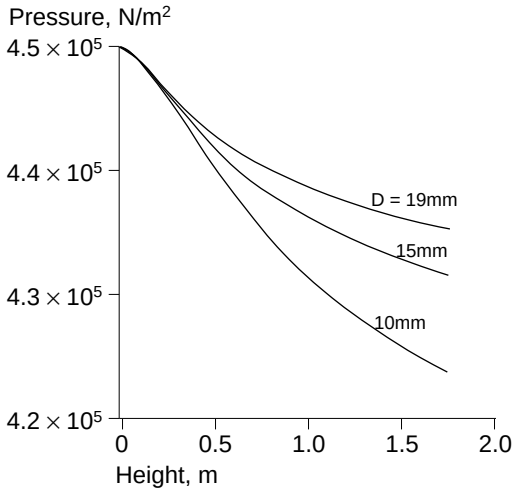

Figure 2.
Variation of pressure with height for different diameters

Figure 4 depicts the variation of volumetric mass transfer coefficient $k_L a$ with the gas flow rate for different liquid flow rates. The volumetric mass transfer coefficient increases with gas flow rate up to a certain maximum and a further increase in gas flow rate leads to a decrease of the value of $k_L a$. At high gas flow rates, the decrease in the value of $k_L a$ can be attributed to the formation of large coalesced bubbles and slugging, which decreases the efficiency of the absorber. Another reason is at high gas flow rates the flow pattern changes to annular flow which possess smaller area for mass transfer. The mass transfer coefficient $k_L a$ increases with increase in liquid velocity up to a limit and followed by a decrease. This reduction is due to the change in flow pattern from annular to annular mist. At high gas velocities the entrained droplets behave like rigid spheres, which reduce mass transfer (Keizer, 1982; Roman Zarzycki and Andrzeg Chacuk, 1993; Shilimkan and Stempanek, 1977).

Figure 5 shows the variation of average heat transfer coefficient with diameter for different gas velocities. As the diameter increases the heat transfer coefficient decreases and for the same diameter, the heat transfer coefficient

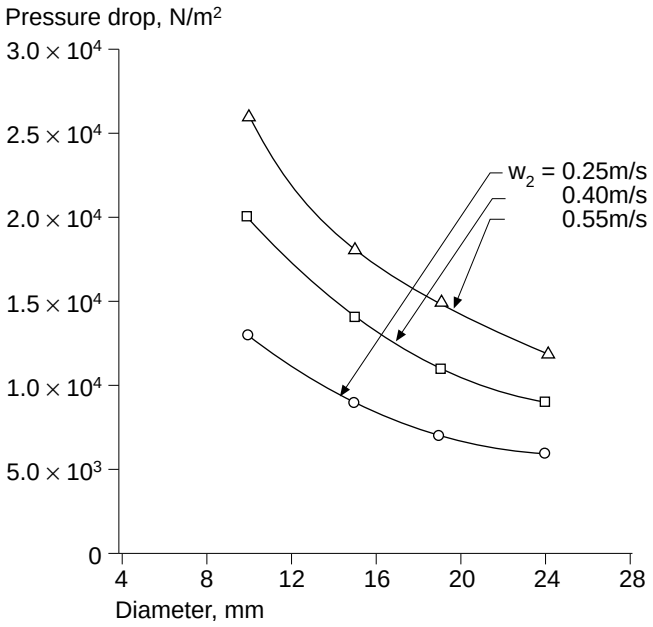

Figure 3.
Variation of pressure drop with diameter for different gas velocities

increases with gas velocity. As the diameter increases the distance between the gas liquid interface where heat of absorption is evolved and the tube wall increases. Thus the resistance to heat transfer increases and the average heat

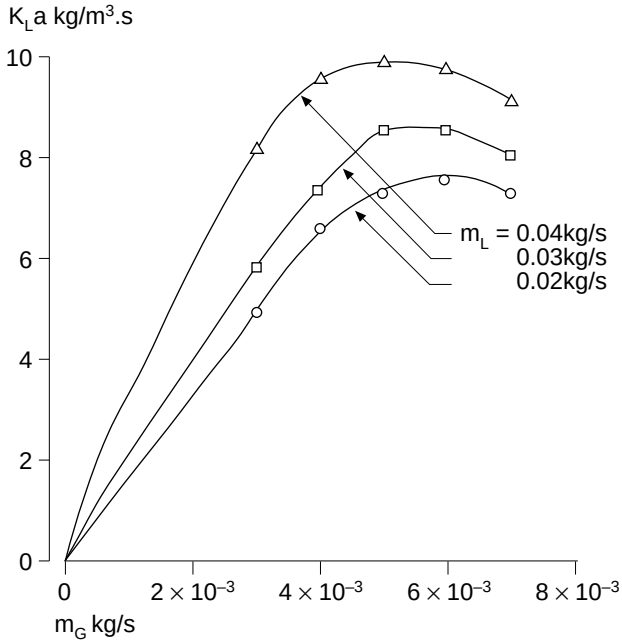

Figure 4.
Variation of volumetric mass transfer coefficient with gas flow rate for different liquid flow rates

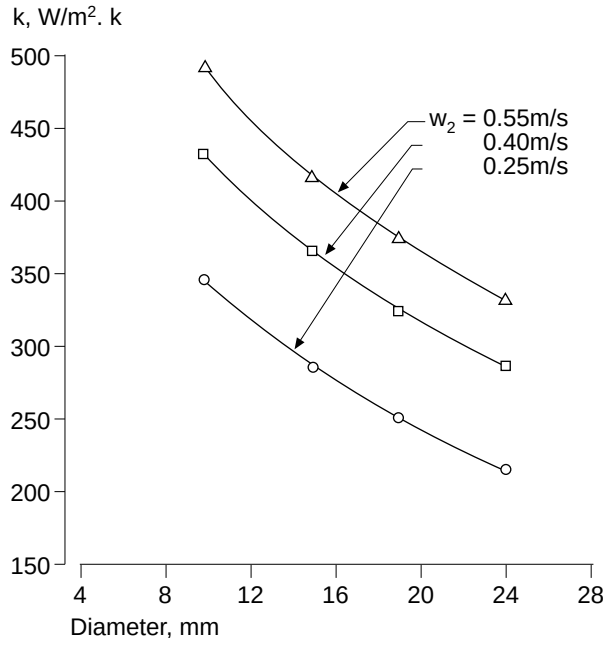

Figure 5.
Variation of average heat transfer coefficient with diameter for different gas velocities

transfer coefficient decreases. Average heat transfer coefficient increases with gas velocity. But as the gas velocity increases pressure drop also increases as shown in Figure 3. Hence it is not preferable to go for high gas velocity to achieve high heat transfer coefficients.

Figure 6 shows the variation of average heat transfer coefficient with coolant flow rate for different diameters. As the cooling water flow rate increases, the heat transfer coefficient increases first gradually and then rapidly. The sudden increase in heat transfer coefficient can be attributed to the change of flow in the annulus from laminar to turbulent. Smallest diameter gives large heat transfer coefficients but causes drastic increase in pressure drop as shown in Figure 2.

Figure 7 shows the variation of void fraction along the height of the absorber for different diameters. As the flow proceeds from the lower end of the absorber, the gas gets absorbed and the gas flow rate decreases. Thus void fraction being the ratio of volume of the gas per unit volume of the solution, decreases.

The performance curves show that the present model is capable of predicting the characteristics of heat and mass transfer in vertical tubular bubble absorbers.

Analysis is done by varying absorber length, diameter, gas flow rate, liquid flow rate, pressure and temperature. By a multiple linear regression analysis of the data, the following correlation is suggested for the vertical tubular bubble absorber with R22-DMF as working fluid:

$$Sh_{VL} = 5.79\ (Re_{L+G})^{0.81}\ (Sc_L)^{0.36}\ (Z/D)^{-0.78} \qquad (20)$$

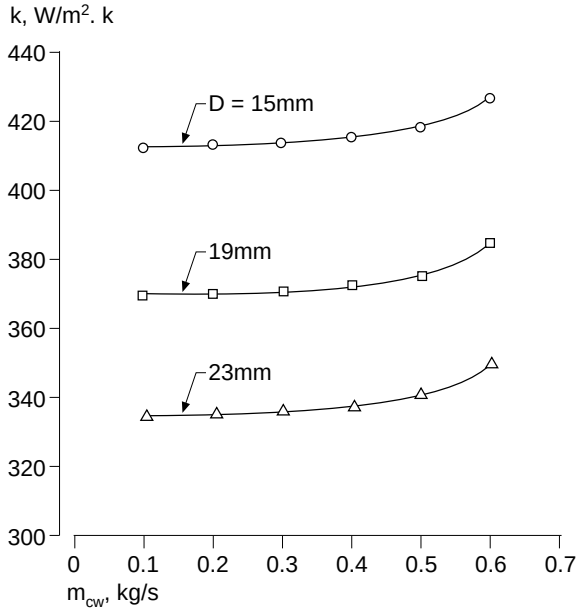

Figure 6.
Variation of average heat transfer coefficient with cooling water flow rate for different diameters

where Sh_{VL} is the volumetric Sherwood number, Re_{L+G} is the Reynolds number, Sc_L is the Schmidt number and Z/D is the length to diameter ratio. Sh_{VL}, Re_{L+G}, and Sc_L are calculated as given in Appendix 2. Figure 8 shows the variation between actual and predicted Sherwood numbers.

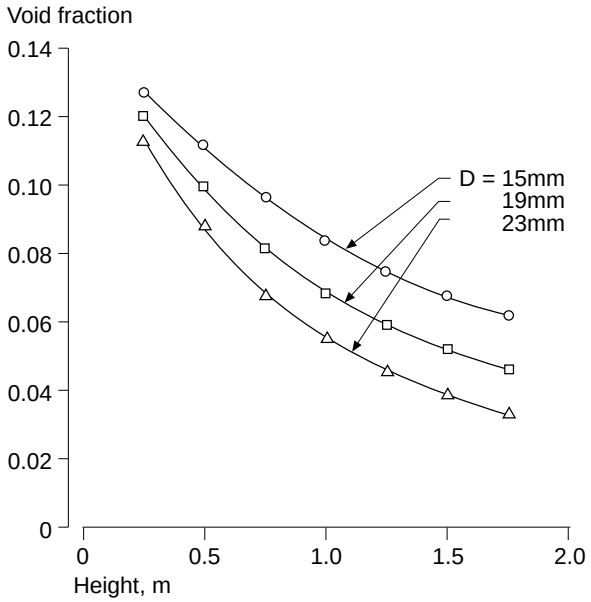

Figure 7.
Variation of void fraction with height for different diameters

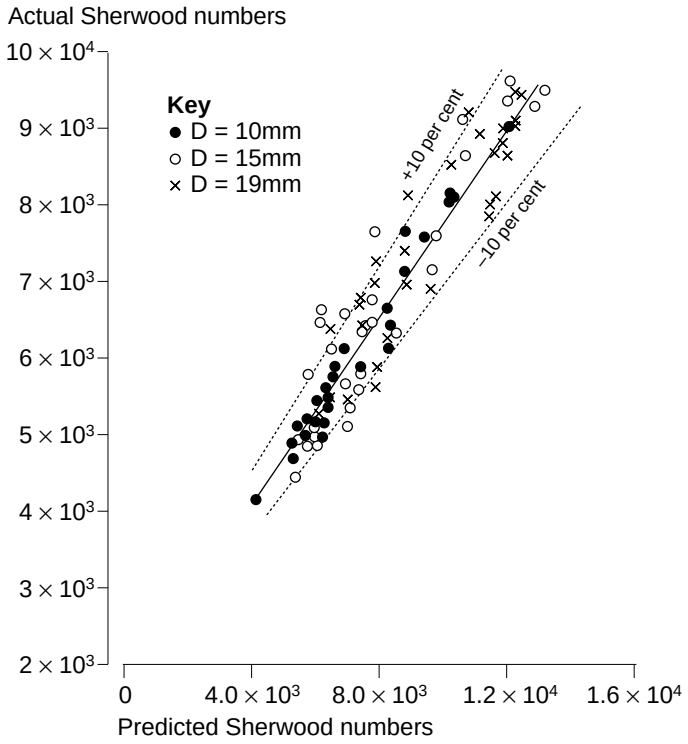

Figure 8.
Variation of actual Sherwood number with predicted Sherwood number

The function of the proposed correlation is for calculating the mass transfer rates or for determining the height required or the diameter of the absorber for a specified mass transfer rate. The criterion for the design can be the mass transfer coefficient, which depends on various parameters (fluid properties, mass flow rates, diameter etc.). A designer can consider a combination of these parameters and select one which suits the practical situation. It is thus convenient to use a single quantity, namely Reynolds number, and a correlation in which it is related to the Sherwood number through the fluid properties.

Conclusions

A vertical tubular bubble absorber working with R22-DMF is analysed numerically using Galerkin's technique. The model is validated by comparing with the results available in the literature. A correlation is suggested for vertical tubular bubble absorber working with R22-DMF, which can be used for design purposes.

References

Collier, J.G. (1980), *Convective Boiling and Condensation*, McGraw-Hill, New York, NY.

Fatouh, M. and Srinivasa Murthy, S. (1993a), "Comparison of R22-absorbent pairs for absorption cooling based on P-T-X data", *J. Renewable Energy*, Vol. 3, pp. 31-7.

Fatouh, M. and Srinivasa Murthy, S. (1993b), "Comparison of R22-absorbent pairs for absorption cooling based on H-T-X data", *J. Renewable Energy*, Vol. 3, pp. 262-71.

Fatouh, M. and Srinivasa Murthy, S. (1993c), "Comparison of R22-absorbent pairs for vapour absorption heat transformers based on P-T-H-X data, *Heat Recovery Ssytems and CHP*, Vol. 13, pp. 33-48.

Gallant, R.W. (1969), "Physical properties of hydrocarbons", *Hydrocarbon Journal*, pp. 199-205.

Infante Ferreira, C.A., Keizer, C. and Michelsen, C.H.M. (1984), "Heat and mass transfer in vertical tubular bubble absorbers for ammonia-water absorption refrigeration system", *Int. J. Refrig.*, Vol. 7, pp. 348-57.

Jagota, A.K., Rhodes, E. and Scott, D.S. (1973), "Mass transfer in upward gas-liquid annular flow", *Chem. Engng. J.*, Vol. 5, pp. 23-31.

Kasturi, G. and Stepanek, J.B. (1974), "Two-phase flow – 1V: gas and liquid side mass transfer coefficients", *Chem. Engng. Sci.*, Vol. 29, pp. 1849-56.

Keizer, C. (1982), "Absorption refrigeration machines", Report, Laboratory of Refrigeration and Indoor Climate Technology, Delft University of Technology, Delft.

Kouremenos, D.A., Stegou-Sagia, A. and Antonopoulos, K.A. (1990), "Heat and mass transfer in the absorber of neutral gas absorption refrigeration units", *Proc. First Int. Conf. on Advanced Computational Methods in Heat Transfer*, Portsmouth, Vol. 2, pp. 389-97.

Kouremenos, D.A., Antonopoulos, K.A., Stegou-Sagia, A. and Rogdakis, E.D. (1993), "Prediction of the irreversible absorption process in annular absorbers with methylamine as refrigerant and hydrogen as inert gas", *Proc. Int. Conf. on Energy Systems and Ecology ENSEC '93*, Cracow, Vol. 1, pp. 245-55.

Prashanth, K.V. and Seetharamu, K.N. (1993), "FEM predictions for two-phase flow in a vertical pipe without the use of any external correlations", *Int. J. Num. Meth. Heat Fluid Flow*, Vol. 3, pp. 565-75.

Roman Zarzycki and Andrzeg Chacuk (1993), *Absorption, Fundamentals and Applications*, Pergamon Press Ltd, Oxford.

Schittke, H.J. (1975), "Berucksichtigung von Druck and Zweiphasen-Impulsaustausch bei der Dynamik eines konvektiv beheizten Zwangdurch-laufdampferzeugers", PhD thesis, University of Stuttgart, December.

Segerlind, L.J. (1984), *Applied Finite Element Analysis*, John Wiley, New York, NY.

Appendix 1

The elements of the stiffness matrix are

$K_{11} = v_j(t)$
$K_{15} = -v_i(t)$
$K_{22} = (2\delta z/\delta t) - [2w_i(t) + w_j(t)]$
$K_{23} = -(\delta z/2\delta t)\,[3v_i(t) + v_j(t)]$
$K_{26} = (\delta z/\delta t) + 2w_i(t) + w_2(t)$
$K_{27} = -(\delta z/2\delta t)\,[v_i(t) + v_j(t)]$
$K_{31} = K_{22}$
$K_{33} = -[2v_i(t) + v_j(t)]$
$K_{35} = K_{26}$
$K_{37} = -K_{33}$
$K_{41} = [2w_i(t) + w_j(t)] - [2w_{1i}(t) + w_{1j}(t)] + (1/2)\,\{[3w_{2i}(t) + w_{2j}(t)]\,[x_j(t) - x_i(t)]\}$
$K_{43} = -[2v_{1i}(t) + v_{1j}(t)]$
$K_{44} = K_{42}$
$K_{45} = [2w_{1i}(t) + w_{1j}(t)] - [2w_i(t) + w_j(t)] + (1/2)\,\{[w_{2i}(t) + w_{2j}(t)]\,[x_j(t) - x_i(t)]\}$
$K_{47} = -K_{43}$
$K_{48} = K_{26}$
$K_{51} = K_{11}$

$K_{55} = K_{15}$
$K_{62} = (\delta z/\delta t) - [w_i(t) + 2w_j(t)]$
$K_{63} = -(\delta z/2\delta t)\,[v_i(t) + v_j(t)]$
$K_{66} = (2\delta z/\delta t) + w_i(t) + 2w_j(t)$
$K_{67} = -(\delta z/2\delta t)\,[v_i(t) + 3v_j(t)]$
$K_{71} = K_{62}$
$K_{73} = -[v_i(t) + 2v_j(t)]$
$K_{75} = K_{66}$
$K_{77} = -K_{73}$
$K_{81} = [w_i(t) + 2w_j(t)] - [w_{1i}(t) + 2w_{1j}(t)] + (1/2)\,\{[w_{2i}(t) + w_{2j}(t)]\,[x_j(t) - x_i(t)]\}$
$K_{83} = -[v_{1i}(t) + 2v_{1j}(t)]$
$K_{84} = K_{62}$
$K_{85} = [w_{1i}(t) + 2w_{1j}(t)] - [w_i(t) + 2w_j(t)] + (1/2)\,\{[w_{2i}(t) + w_{2j}(t)]\,[x_j(t) - x_i(t)]\}$
$K_{87} = -K_{83}$
$K_{84} = K_{62}$

All other elements are zeros

$f_1 = -(\delta z/3\delta t)\,\{[2v_i(t) + v_j(t)] - [2v_i(t_0) + v_j(t_0)]\}$
$f_2 = [2v_i(t) + v_j(t)]\,Q.\delta z - (\delta z/2\delta t)\,\{[3v_i(t) + v_j(t)]\,p_i(t_0) + [v_i(t) + v_j(t)]\,p_j(t_0)\}$
$f_3 = -3g.\sin\Psi.\delta z - \delta z(2fw_i^2 + fw_j^2) + (\delta z/\delta t)\,[2w_i(t_0) + w_j(t_0)]$
$f_4 = F_1 - F_2$
$F_1 = (\delta z/\delta t)\,[2w_{1i}(t_0) + w_{1j}(t_0)] - 3g.\sin\Psi.\delta z - \delta z(2f_1w_{1i}^2 + f_1w_{1j}^2)$
$F_2 = (\delta z/2\delta t)\,\{[3w_{2i}(t) + w_{2j}(t)]\,[x_i(t) - x_i(t_0)] + [w_{2i}(t) + w_{2j}(t)]\,[x_j(t) - x_j(t_0)]\}$
$f_5 = -(\delta z/3\delta t)\,\{[v_i(t) + v_j(t)] - [v_i(t_0) + 2v_j(t_0)]\}$
$f_6 = [v_i(t) + 2v_j(t)]\,Q.\delta z - (\delta z/2\delta t)\,\{[v_i(t) + v_j(t)]\,p_i(t_0) + [v_i(t) + 3v_j(t)]\,p_j(t_0)\}$
$f_7 = -3g.\sin\Psi.\delta z - \delta z(fw_i^2 + 2fw_j^2) + (\delta z/\delta t)\,[w_i(t_0) + 2w_j(t_0)]$
$f_8 = F_3 - F_4$
$F_3 = (\delta z/\delta t)\,[w_{1i}(t_0) + 2w_{1j}(t_0)] - 3g.\sin\Psi.\delta z - \delta z(f_1w_{1i}^2 + 2f_1w_{1j}^2)$
$F_4 = (\delta z/2\delta t)\,\{[w_{2i}(t) + w_{2j}(t)]\,[x_i(t) - x_i(t_0)] + [w_{2i}(t) + 3w_{2j}(t)]\,[x_j(t) - x_j(t_0)]\}$

$\Phi(t)$ represents the value of Φ at the present time step and $\Phi(t_0)$ represents the value of Φ at the previous time step where Φ represents any property.

Appendix 2. Calculation of heat and mass transfer coefficients

Mass transfer coefficient

An element of length δz of the tubular absorber is shown in Figure A1. Mass flux is calculated using the relation

$$m = G\,\beta \tag{21}$$

β is the driving force and G is the conductance. The relation for mass transfer driving force is given by Spalding (1963) in terms of temperatures or enthalpies. $\beta = \delta h/q$, where δh is the enthalpy difference between the neighbouring phase and the considered phase and q is the heat

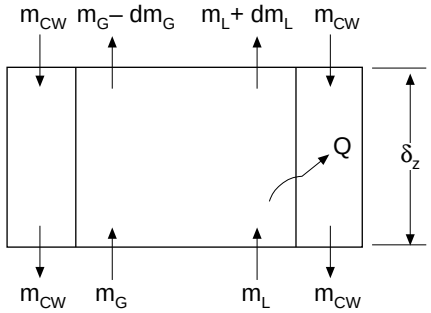

Figure A1.
An element of the tubular absorber

transfer through the interface per unit mass transfer. The relation for conductance is taken from Spalding(1963). From these, the mass transferred dm_G can be calculated.

Law of conservation of mass applied on an element gives

$$m_G + m_L = (m_G - dm_G) + (m_L + dm_L) \tag{22}$$

From the mass balance of the R22 component

$$m_G\, \xi_G + m_L\, \xi_L = (m_G - dm_G)\, \xi_G + (m_L + dm_L)(\xi_L + d\, \xi_L) \tag{23}$$

where ξ_G is the concentration of R22 in the gas and ξ_L is the concentration of R22 in the liquid. From the above relation the increase in concentration $d\xi_L$ can be calculated. The mass transfer coefficient $k_L a$ can be calculated from the relation

$$dm_G = -k_L\, a\, (\xi_L^* - \xi_L)\, dv = -k_L\, a\, (\xi_L^* - \xi_L)\, \pi\, D^2\, \delta z / 4 \tag{24}$$

where ξ_L^* represents the equilibrium concentration and is calculated from Fatouh and Srinivasa Murthy (1993a). Void fraction α is calculated using the relation given in Collier (1980) and Prashanth and Seetharamu (1993).

Overall heat transfer coefficient

The cooling water flows counter current to the flow of gas and liquid. The overall heat transfer coefficient k is calculated using the relation

$$Q = k\, A\, \delta T_{1n} \tag{25}$$

where δT_{1n} is the logarithmic mean temperature difference. Q is the quantity of heat transferred to the coolant. This is the sum of heat of absorption and heat of condensation.

Calculation of Sh_{VL}, Re_{L+G} and Sc_L

Sherwood number, Reynolds number and Schmidt number are calculated using the following equations (Keizer, 1982).

$$Sh_{VL} = \frac{k_L a\, D^2}{\rho_L\, Dc} \tag{26}$$

$$Re_{L+G} = \frac{4\, \rho_L \left(\dfrac{m_L}{\rho_L} + \dfrac{m_G}{\rho_G} \right)}{\pi\, D\, \mu_L} \tag{27}$$

$$Sc_L = \frac{\nu_L}{Dc_L} \tag{28}$$